Theoretical Notes
Note 217

DNA 3602T

EMP GENERATION NEAR OBJECTS WITH CYLINDRICAL SYMMETRY IN THE SOURCE REGION

R & D Associates
P.O. Box 3580
Santa Monica, California 90403

Charles T.C. Mo

19 June 1975

Topical Report

CONTRACT No. DNA 001-74-C-0139

THIS WORK SPONSORED BY THE DEFENSE NUCLEAR AGENCY
UNDER SUBTASK P99QAXDB001-13.

Prepared for
Director
DEFENSE NUCLEAR AGENCY
Washington, D. C. 20305

SUMMARY

In this report we have

(1) changed the numerical code ONDINE into a numerical code RONDINE to compute the EMP fields in a source region surrounding a conducting wire whose axis is parallel to the γ-ray flux, with the average self-consistency deflection of the Compton current shown to be an important effect and taken into account;

(2) analyzed the circular cylindrical source region problem and obtained formal solutions and simple approximate formulas for the conducting wire in a source region;

(3) obtained numerical results for a typical conducting wire problem from RONDINE and from the simple analytical formulas and shown their agreement when the self-consistency correction is ignored;

(4) and spelled out the very minor differences between RONDINE and the coaxial source region case, and between the RONDINE and the underground test EMP prediction.

These results apply when a cylindrical structure is immersed in the source region and has its axis parallel to the γ-flux of the nuclear burst. Such analysis also applies to any structure of revolution when the axis of revolution is parallel to the incident source flux and the skin depth of the environment is much smaller than the axial length of the structure. One interesting example of such a situation is a missile flying away or toward an explosion in the source region. RONDINE is applicable for the first one-tenth of a millisecond when the conductivity is high and skin depth small. For later times, a steady-state [8] analysis sets an upper limit to the charge and current induced on the missile surface. For very early times with very low conductivity ($\tau - \tau_o < 10^{-9}$ sec), the problem is a scattering of the longitudinal field $E_{zo}(\tau)$ by the missile. But then the incident field and the Compton current are too small to cause any current or field compared with later

peak values. Other problems for which these results are applicable include the EM coupling to power and communication lines in the source region, underground EMP test geometries having cylindrical symmetry.

PREFACE

Many helpful discussions with Dr. W. R. Graham, Mr. R. R. Schaefer, and Dr. L. Schlessinger, and valuable suggestions from Major W. E. Adams are acknowledged with pleasure.

TABLE OF CONTENTS

LIST OF ILLUSTRATIONS

SECTION 1
INTRODUCTION

It has long been recognized that the electromagnetic (EM) source terms in the region close to a nuclear explosion consist of Compton and photoelectric currents and collision-induced conductivity [1]. These source terms create a pulse of EM field (EMP) both in the region itself and outside the source region [2]. For an object outside the source region, the EMP effect is produced through free-field coupling [3]. For an object inside the region, the EMP effect should be obtained by solving the boundary value problem using the current and the conductivity directly as the driving source.

In this work, we determined the EMP effect on a circular cylindrical structure oriented parallel to the source fluxes in the source region. This analysis applies for the following cases: (1) a conducting wire immersed in the source region; (2) a wire above conducting ground with a height greater than the skin depth in the environment such that the ground can approximately be considered coaxially wrapped around the wire; and (3) any object of revolution when the environment's skin depth is much smaller than the axial length of the object, when in the region of interest the photon flux has negligible attenuation and the surrounding medium does not change along the axis.

In Section 2, we first obtain a numerical code RONDINE for the circular cylindrical source region problem by slightly modifying an established and tested one-spatial-dimensional planar code ONDINE [4]. RONDINE is applicable to any circular cylindrically-stratified driving current source, air conductivity, and geometry, subject only to the limitation that the spatial variation along the cylindrical z-axis and the temporal variation t for the whole problem is through the dependence of

$$\tau \equiv t - z/c \qquad (1\text{-}1)$$

where c is the velocity of light in the soruce region. Physically, this ignores the attenuation along the z-axis of the γ-flux and x-rays, and, therefore, such attenuation of the driving current and the ionization conductivity. Thus, all points of different z are identical except that they experience a time-shifted driving source and EM responses. Such an approximation holds when the ionization conductivity σ of the environment is high enough to shield the EM effects at two points from each other if they are spaced $\gtrsim \lambda$ apart, i.e., when

$$\lambda >> \delta \tag{1-2}$$

Here $\lambda \equiv$ mean free path of the photons giving rise to the EMP source terms and the skin depth δ is

$$\delta = \begin{cases} \dfrac{\sqrt{2}}{\sqrt{\omega\mu\sigma}} & \text{if } \sigma >> \omega\varepsilon \\ \dfrac{\sqrt{2}}{\sqrt{\mu/\varepsilon}\ \sigma} & \text{if } \sigma << \omega\varepsilon \end{cases} \tag{1-3}$$

In the above, ω is the dominant angular frequency of the driving current, and μ and ε are, respectively, the magnetic permeability and the dielectric constant of the source region.

Next, we use RONDINE to compute the typical case of the wire in a source region, without and with self-field correction to the driving current, and show that self-field effects can substantially reduce the current induced in the wire.

Then, in Section 3, we analytically solve the cylindrical wire problem and the cylindrical coaxial wire problem. The analytical expressions can be reduced to simple formulas under various approximations. Such formulas for a wire are then evaluated and compared with the RONDINE results in Section 2. These show very good agreement.

Finally, we briefly discuss the application of RONDINE to an underground test and conclude with a short summary.

SECTION 2

THE NUMERICAL CODE RONDINE

2.1 The Maxwell equations.

Figure 1 shows a perfectly conducting cylinder of radius R in a source region with its z-axis along the direction of the γ-ray (and/or x-ray) propagation of a nuclear explosion. Under the approximations discussed for (1-1) to (1-3), the driving (Compton and/or photoelectric) current is

$$\underset{\sim}{J}_{\text{driving}} = \underset{\sim}{e}_z J_z(\tau,\rho) + \underset{\sim}{e}_\rho J_\rho(\tau,\rho) \tag{2-1}$$

and the induced air conductivity is $\sigma(\tau,\rho)$. Notice that the $J_\rho(\tau,\rho) \equiv 0$ if we ignore the influence of the wire's fields on the driving current.

Now the ϕ-symmetry makes $E_\phi = 0$. Therefore, the only non-vanishing fields are $E_\rho(\tau,\rho)$, $E_z(\tau,\rho)$ and $H_\phi(\tau,\rho)$, which obey the Maxwell equations:

$$\frac{1}{c}\frac{\partial}{\partial\tau} E_\rho + \frac{\partial}{\partial\rho} E_z = \mu \frac{\partial H_\phi}{\partial\tau} \tag{2-2}$$

$$\frac{1}{c}\frac{\partial}{\partial\tau} H_\phi = \sigma E_\rho + \varepsilon\frac{\partial E_\rho}{\partial\tau} + J_\rho \tag{2-3}$$

$$\frac{1}{\rho}\frac{\partial}{\partial\tau} (\rho H_\phi) = \sigma E_z + \varepsilon\frac{\partial E_z}{\partial\tau} + J_z \tag{2-4}$$

These imply the "equation for H":

$$\frac{\partial}{\partial\rho}\left[\frac{1}{\rho}\frac{\partial}{\partial\rho} (\rho H_\phi)\right] - \mu\sigma\frac{\partial}{\partial\tau} H_\phi = \frac{\partial J_z}{\partial\rho} + \frac{1}{c}\frac{\partial J_\rho}{\partial\tau} + E_z\frac{\partial\sigma}{\partial\rho} + \frac{E_\rho}{c}\frac{\partial\sigma}{\partial\tau} \tag{2-5}$$

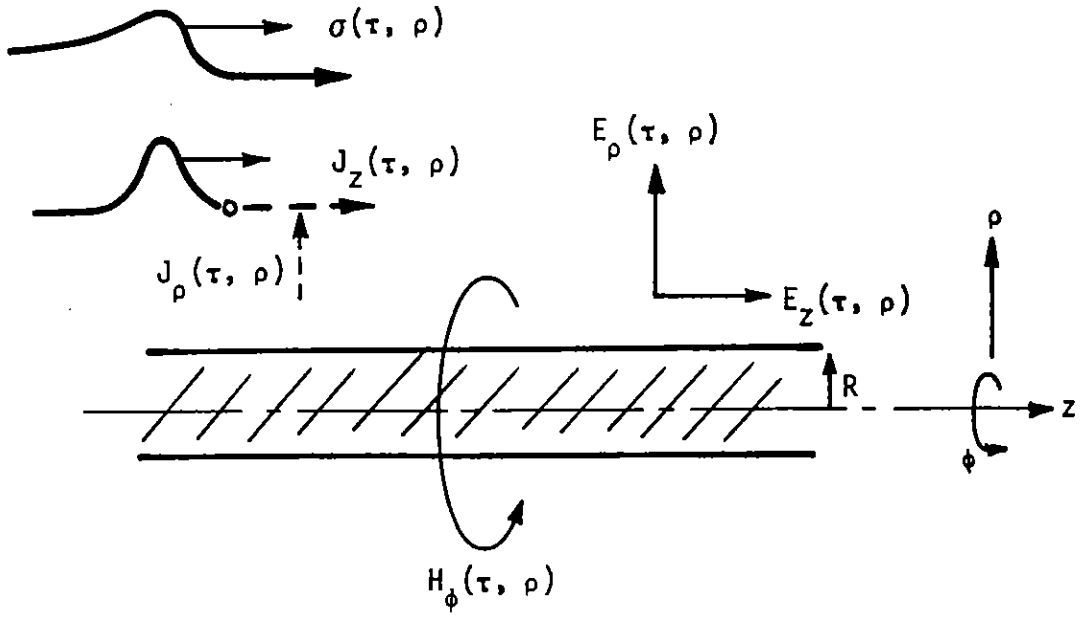

Figure 1. The cylindrical geometry of a conducting wire in the source region for RONDINE, $\tau \equiv t - z/c$.

The boundary conditions for E_z are

$$E_z(\tau,R) = 0, \quad E_z(\tau,\rho\to\infty) \to E_{zo}(\tau) \tag{2-6}$$

where

$$E_{zo}(\tau) \equiv - e^{-\int_o^\tau \frac{\sigma_o(\tau')}{\varepsilon} d\tau'} \int_o^\tau d\tau' \frac{J_{zo}(\tau')}{\varepsilon} e^{\int_o^{\tau'} \frac{\sigma_o(\tau'')}{\varepsilon} d\tau''} \tag{2-7}$$

is the electric field, $\sigma_o(\tau)$ is the conductivity, and $J_{zo}(\tau)$ is the driving current without the presence of the wire. The σ and $\underset{\sim}{J}$ differ from σ_o and J_{zo} in that they are modified by the fields caused by the presence of the wire. This effect is treated in RONDINE by a perturbation or normalization at each time step. Also, from (2-6), the boundary conditions for H_ϕ are

$$\left(\frac{1}{\rho}\frac{\partial}{\partial\rho}(\rho H_\phi)\right)_{\rho=R} = J_z(\tau,R), \quad \left(\frac{1}{\rho}\frac{\partial}{\partial\rho}(\rho H_\phi)\right)_{\rho\to\infty} = 0 \tag{2-8}$$

2.2 The finite difference scheme.

To make use of ONDINE [4], the finite difference scheme used in this report for the fields is precisely the same as that used in Reference 4. Namely, it is an implicit 1/2, 1/2 scheme in time steps to obtain a set of tridiagonal equations for H_ϕ [5]. This set of equations is inverted with the help of the boundary conditions (2-8), where a $\rho = \rho_\infty$ satisfying

$$\rho_\infty >> \text{minimum } [c\tau_{max}, \text{ maximum } (\delta,R)] \tag{2-9}$$

is used to replace the $\rho \to \infty$ theoretical outer boundary such that the answer is not sensitive to any particular choice of ρ_∞. The τ_{max} is the

maximum time elapse within which we are interested in the numerical integration. The exact derivation of the finite difference equations is almost the same as that in ONDINE. (We refer interested readers to Reference 4 for such details.)

Now we change the notations in (2-2) through (2-4) and (2-8) into the same notations that were used in ONDINE:

$$
\begin{aligned}
(\rho,\phi,z) &\rightarrow (Z,-Y,X) \\
E_\rho &\rightarrow e_Z \\
E_z &\rightarrow e_X \\
H_\phi &\rightarrow -h_Y \\
J_\rho &\rightarrow j_Z \\
J_z &\rightarrow j_X
\end{aligned}
\tag{2-10}
$$

Then setting the incident angle $\theta = 0$ in ONDINE makes the equations for RONDINE the same as those for ONDINE, except the ones caused by (2-4) and (2-8).

To obtain these changes, we first realized from analysis (see Section 3) that H_ϕ will behave approximately as $\sim 1/\rho$ for ρ near the wire. But from (2-5), this results in a near cancellation among the large terms of the spatial operator in the left-hand side of (2-5). This then demands small time steps near the wire to avoid possible oscillations in the results, and severely limits the maximum time in which we can carry out the integration without using a set of elaborate spatially dependent time-grid sizes. One way to overcome this problem is to explicitly extract the $1/\rho$ dependence and solve for

$$
\tilde{H}_\phi \equiv \rho H_\phi \tag{2-11}
$$

instead of H_ϕ, and only in the output print out $\tilde{H}_\phi/\rho = H_\phi$. Incidentally, solving for $\tilde{H}_\phi$ instead of H_ϕ tremendously simplifies the differences

between the codes RONDINE and ONDINE into virtually trivial ones. The resulting changes are replacing the lowest grid boundary condition at p.35 of ONDINE by

$$E_1 = 1$$
$$F_1 = j_X(1)\ (\Delta Z)_{1\,2}\ \frac{Z(1) + Z(2)}{2} \qquad (2\text{-}12)$$

and replacing the coefficients A_3, B_1, C_1, C_2 in ONDINE by the following

$$A_3 \to -\mu' \cdot \frac{2}{Z(j) + Z(j+1)}$$

$$B_1 \to -(1-e^{-K\Delta\tau}) \cdot \frac{1}{\varepsilon' K\Delta\tau} \cdot \frac{2}{Z(j) + Z(j+1)}$$

$$C_1 \to -(1-e^{-K\Delta\tau}) \cdot \frac{c}{\varepsilon' K\Delta Z} \cdot \frac{2}{Z(j) + Z(j+1)}$$

$$C_2 \to +(1-e^{-K\Delta\tau}) \cdot \frac{c}{\varepsilon' K\Delta Z} \cdot \frac{2}{Z(j) + Z(j+1)} \qquad (2\text{-}13)$$

Here $K \equiv \sigma/\varepsilon$, and $\varepsilon' \equiv \varepsilon/\varepsilon_o$ and $\mu' \equiv \mu/\mu_o$ relative to vacuum. Further, the consistent use of $e_x \equiv o$ at the lowest grid should be imposed, instead of calculating it from the difference formula which involves discreetness and round-off errors.

2.3 Typical results for a conducting wire.

Figures 2 and 4 plot the numerical results from RONDINE (see Appendix B) for a typical wire with a radius R = 1 cm in the source region at a distance of 300 meters from a 10^3 kiloton explosion. Figure 2 shows the early rising time behavior. For comparison, the curve from the first-order theoretical formula is also shown (see Section 3 for an explanation). Figures 3 and 4 continue the later time behaviors of Figure 2. Notice that the $\sigma(\tau,\rho)$ is field dependent and is obtained from the air chemistry subroutine COND [4].

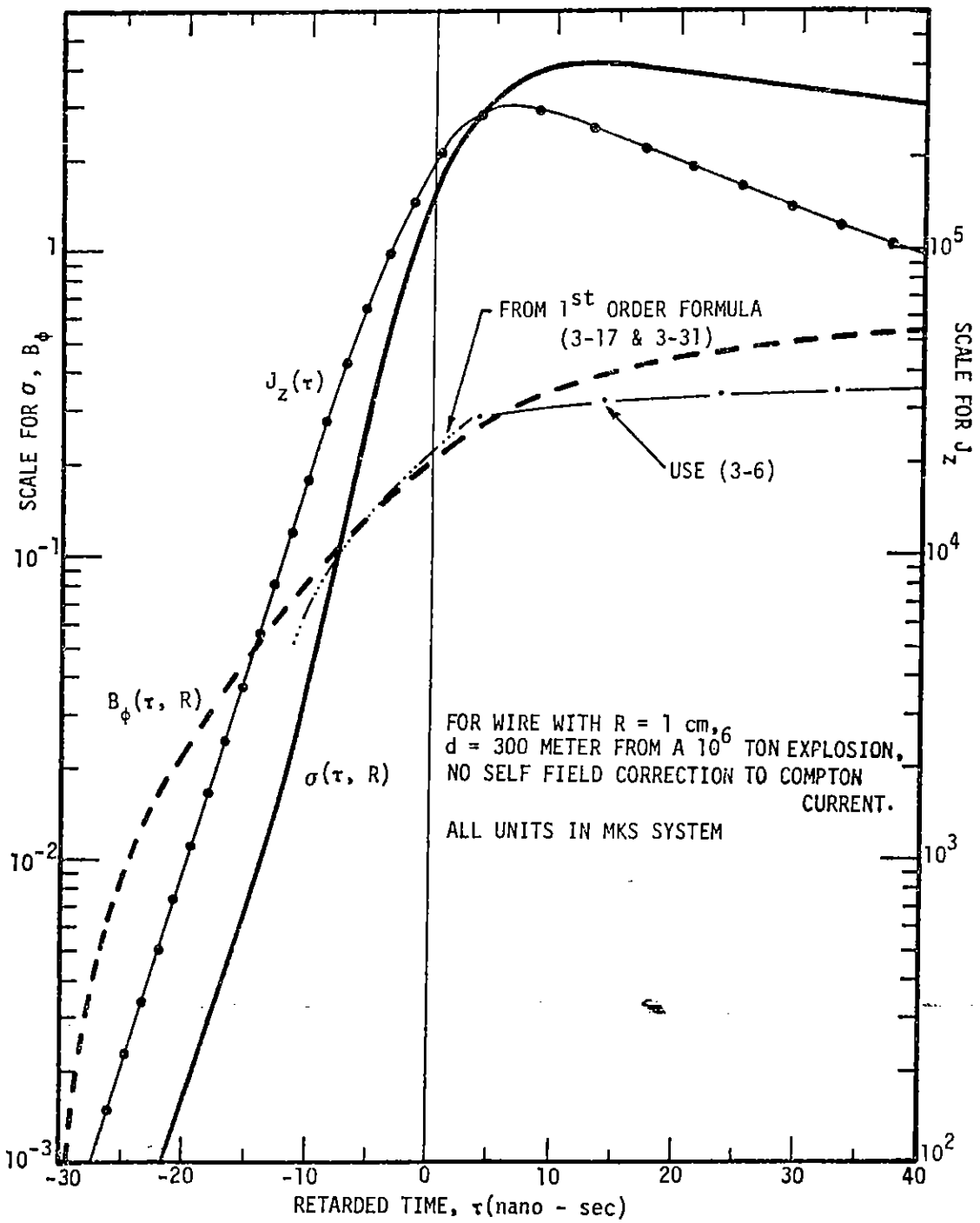

Figure 2. Early time behavior $J_z(\tau)$, $\sigma(\tau,R)$ and $B_\phi(\tau,R)$ without self-consistency from RONDINE.

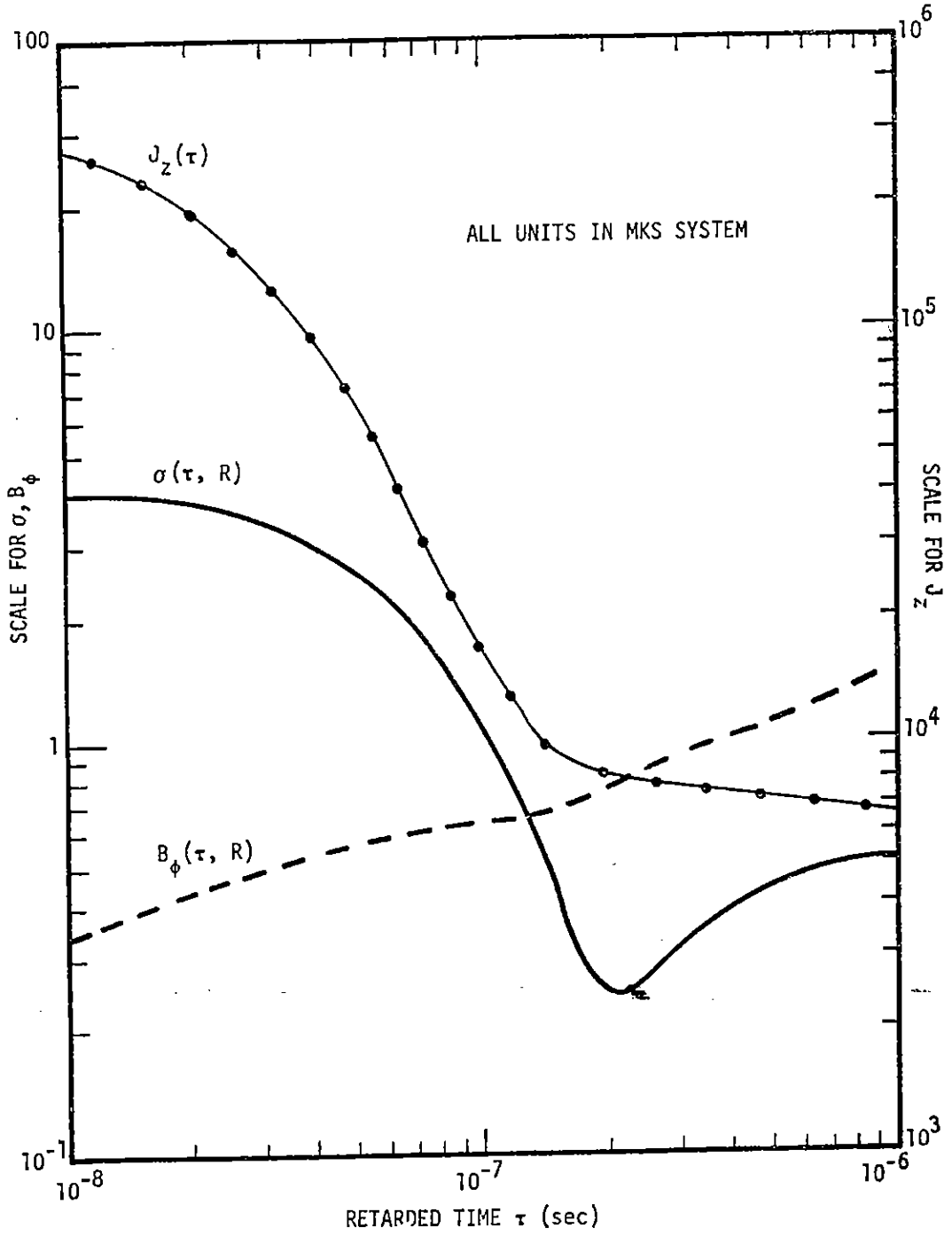

Figure 3. Continuation of Figure 2.

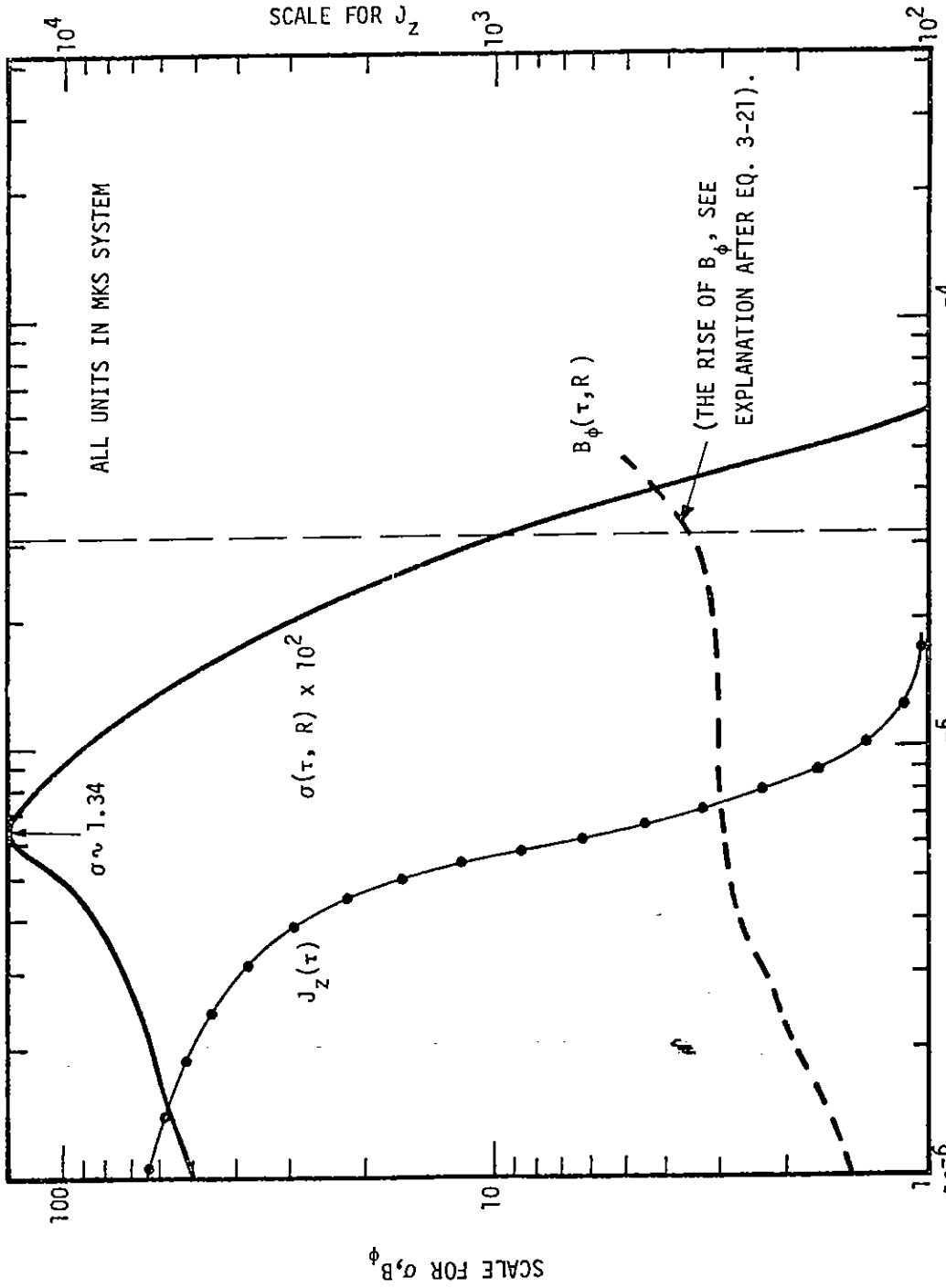

Figure 4. Continuation of Figure 3.

Notice that the late time B_ϕ or wire current increase is caused by the slow decay of J_z (contributed by capture gamma rays from thermal neutrons) at $\sim 3 \times 10^{-5}$ sec, the decreasing of σ, and the fact that any current on the wire after $\underset{\sim}{J} \equiv 0$ decays extremely slowly (see Section 3.3) for explanation). If we truncate the driving current $J_z(\tau \gtrsim 4 \times 10^{-5}$ sec) $\equiv 0$, then the backflow current on the wire

$$I \equiv 2\pi R \cdot \frac{B_\phi}{\mu} = 5 \times 10^6 \, R \text{ (meter)} \cdot B_\phi \text{ (weber/meter}^2\text{)} \qquad (2\text{-}14)$$

can reach a peak of 2×10^5 amp producing ~ 4 weber/meter^2 on the 1-cm radius wire at about $\tau \sim 4 \times 10^{-5}$ sec.

2.4 Lorentz force turning of the Compton electrons and typical results.

Now let us examine the effects of the wire's field on the Compton driving current, the effects we have ignored up to now.

First, the E_ρ deflects the Compton electrons toward the wire when > 0 and away from it when < 0. To estimate such deflections, we examine an electron moving with β_o in the z-direction (see Figure 1). As a result of E_ρ, the ratio of ρ-displacement to z-displacement in its life-time is

$$\frac{\Delta\rho}{\Delta z} \sim \frac{eE_\rho \sqrt{1 - \beta_o^2}\, t}{2m\, V_o}$$

$$\sim \frac{eE_\rho \sqrt{1 - \beta_o^2}\, R_e}{2m\, V_o^2} = 0.98 \times 10^{-6} \frac{\sqrt{1 - \beta_o^2}}{\beta_o^2} R_e \text{ (meter)}$$

$$t \sim \frac{R_e}{V_o}$$

$$\cdot E_\rho \text{ (volt/meter)} \qquad (2\text{-}15)$$

Thus, for an electron of kinetic energy ~ 1 MeV and range $R_e \sim 1.5$ meter in surface atmosphere, the deflection ratio

$$\frac{J^E_{c\rho}}{J^E_{cz}} \sim \frac{\Delta\rho}{\Delta z} \sim 0.4 \times 10^{-6}\ E_\rho \ \text{(volt/meter)} \tag{2-16}$$

is very small for a typical $E_\rho \lesssim 10^4$ volt/meter even near the wire. Thus, we neglect the deflection caused by E_ρ. Here J^E_c and J^E_{cz} are, respectively, the E-field deflected Compton currents in ρ and z directions.

As to the magnetic deflection caused by B_ϕ, we examine the averaged path distortion of a Compton electron in B_ϕ. If we assume that the primary Compton electrons are making inelastic Coulomb collisions along their paths in the z-direction when there is no B_ϕ-deflection according to

$$\text{Probability \{reaching distance} \geq z\} = e^{\frac{-z}{R_e}} \tag{2-17}$$

and that the no-deflection J_{zo} Compton current is obtained from

$$J_{zo} \sim \Delta z_o \sim \text{average \{z-distance travelled\}} = \int_o^\infty z\ \frac{e^{-z/R_e}}{R_e}\, dz = R_e, \tag{2-18}$$

then with B_ϕ present we have the corrected primary current

$$\frac{J_z}{J_{zo}} \sim \frac{\overline{\Delta z}}{\overline{\Delta z}_o} = \frac{\int_o^\infty ds\ \frac{e}{R_e}^{-s/R_e} \cdot r_o \sin\frac{s}{r_o}}{R_e} = \frac{\left(\frac{R_e}{r_o}\right)}{1+\left(\frac{R_e}{r_o}\right)^2} \tag{2-19a}$$

$$\frac{J_\rho}{Jz_o} \sim \frac{\overline{\Delta\rho}}{\overline{\Delta z}_o} = \frac{\int_o^\infty ds\ \frac{e}{R_e}^{-s/R_e} \cdot (r_o - r_o\cos\frac{s}{r_o})}{R_e} = \frac{\left(\frac{R_e}{r_o}\right)}{1+\left(\frac{R_e}{r_o}\right)^2} \tag{2-19b}$$

Here r_o is the Larmour radius of the electron

$$r_o \equiv \frac{mV_o}{eB\phi\sqrt{1-\beta_o^2}} \tag{2-20}$$

and we have used the simple assumption that the electron is on a circular orbit before it is "removed" from the primary stream by a probabilistic collision. Again, for an electron with $\sim$ 1 MeV and $R_e \sim 1.5$ meters, the factor

$$\frac{R_e}{r_o} = 0.587 \cdot 10^3 \cdot \frac{\sqrt{1-\beta_o^2}}{\beta_o} \cdot R_e(\text{meter}) \cdot B_\phi(\text{weber/meter}^2) \tag{2-21}$$

is $\sim 3.11 \times 10^2\ B_\phi$. For a typical wire of 1 cm, the peak B_ϕ near the wire is $\sim$ 1 to 10 weber/meter^2, and the R_e/r_o which is $\sim 10^2$ to 10^3 is not negligible. We thus include the B_ϕ-correction to the Compton current in RONDINE by using (2-19).

Before showing the B_ϕ-corrected RONDINE results, we must point out that the probabilistic distribution (2-17) is very crude. It may not accurately represent the electron penetration in matter, especially near the beginning of small z/R_e, as some readers may have recognized. However, we are only interested in the average displacement an electron travels in its lifetime, with and without B_ϕ-deflection. Since the correct R_e is used in the collisional loss to give a sensible $\mathcal{F}_{zo}$ by the distance-averaging process (2-18), it must also give a relatively sensible B_ϕ-correction to the current by a similar averaging process (2-19). In fact, if we use a more realistic distribution

$$\text{Probability}\{\text{reach} \geq z\} = e^{-\left(\frac{\sqrt{\pi}\, z}{2R_e}\right)^2} \tag{2-22}$$

the resulting correction

$$\frac{J_z}{J_{zo}} \sim e^{-\left(\frac{R_e}{\sqrt{\pi}\, r_o}\right)^2} \qquad (2\text{-}23)$$

does not differ too much from (2-19) if the R_e/r_o is not much greater than one when the corrected B_ϕ is used for the r_o.

The same typical problem for a wire in Section 2.3 is computed again by RONDINE, but with the B_ϕ-correction (2-19) included. The results are plotted in Figures 5, 6, and 7. The current on the wire and H_ϕ field are smaller, as they should be, because from (2-3) the deflected J_ρ (< 0, electrons turning away from the wire) reduces the effect of the σE_ρ (> 0 when building up) and reduces the growth of H_ϕ. The B_ϕ has a weak relative peak of ~ 0.35 weber/meter^2 on the wire at $\tau \sim 8.1 \times 10^{-8}$ sec, and clearly reaches its peak (because of the $\pm$ fluctuation of E_ρ) earlier than the without B_ϕ-correction case with a peak $B_\phi \sim 3.0 \times 10^{-1}$ at $\sim 2.0 \times 10^{-5}$ sec. Again, the late growth ($\tau \gtrsim 3 \times 10^{-5}$) of B_ϕ is caused by the slow diminishing of J, combined with the decay of σ (see Section 3.3). The peak B corresponds to $I \sim 1.5 \times 10^4$ ampere on the wire. Thus, the effect of turning reduces the wire currents by about an order of magnitude.

Finally, a remark on when RONDINE predictions are valid. It is correct for and up to times such that (2-9) holds, that approximations (1-1) and (1-2) are valid, that the height of the wire above the ground is greater than the skin depth such as to justify the cylindrical structure, and that one has confidence in his input driving current and conductivity. Further, possible effects of electric breakdown of the air or insulation surrounding the wire are not included in the present study. Such breakdown may occur at extremely early times for thin wires,

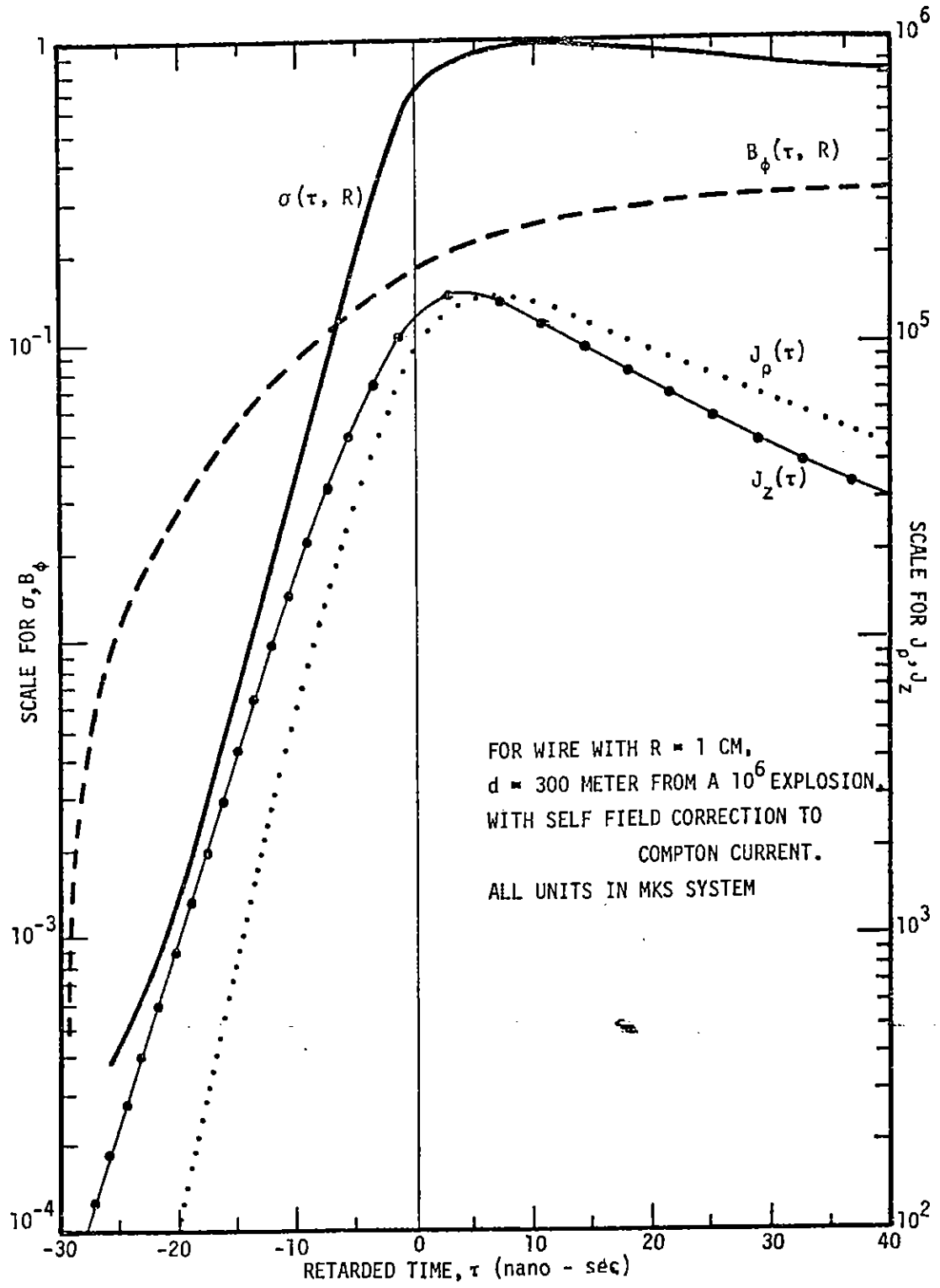

Figure 5. Early time behavior of $\underset{\sim}{J}(\tau)$, $\sigma(\tau,R)$ and $B_\phi(\tau,R)$, with self-magnetic correction, from RONDINE.

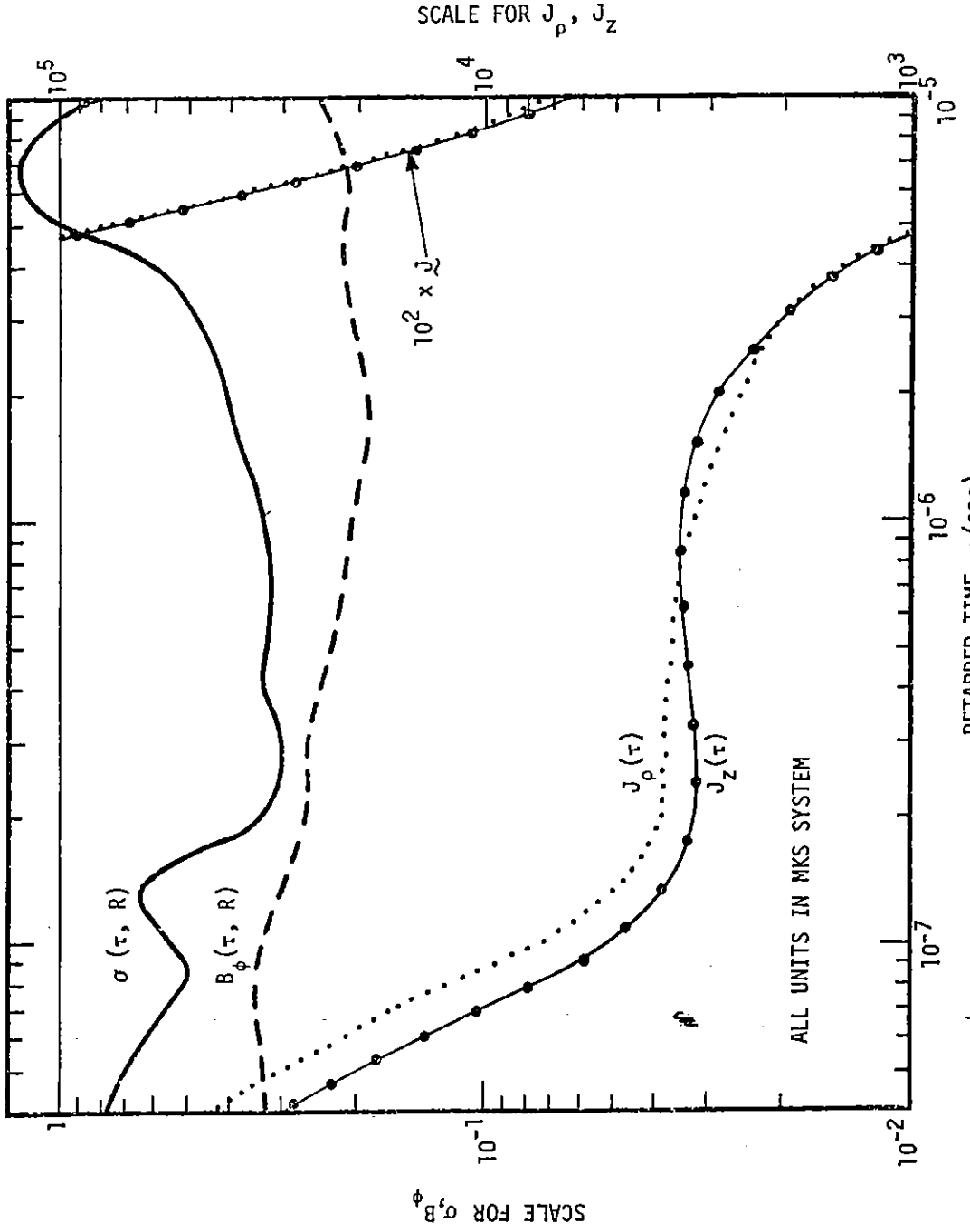

Figure 6. Continuation of Figure 5.

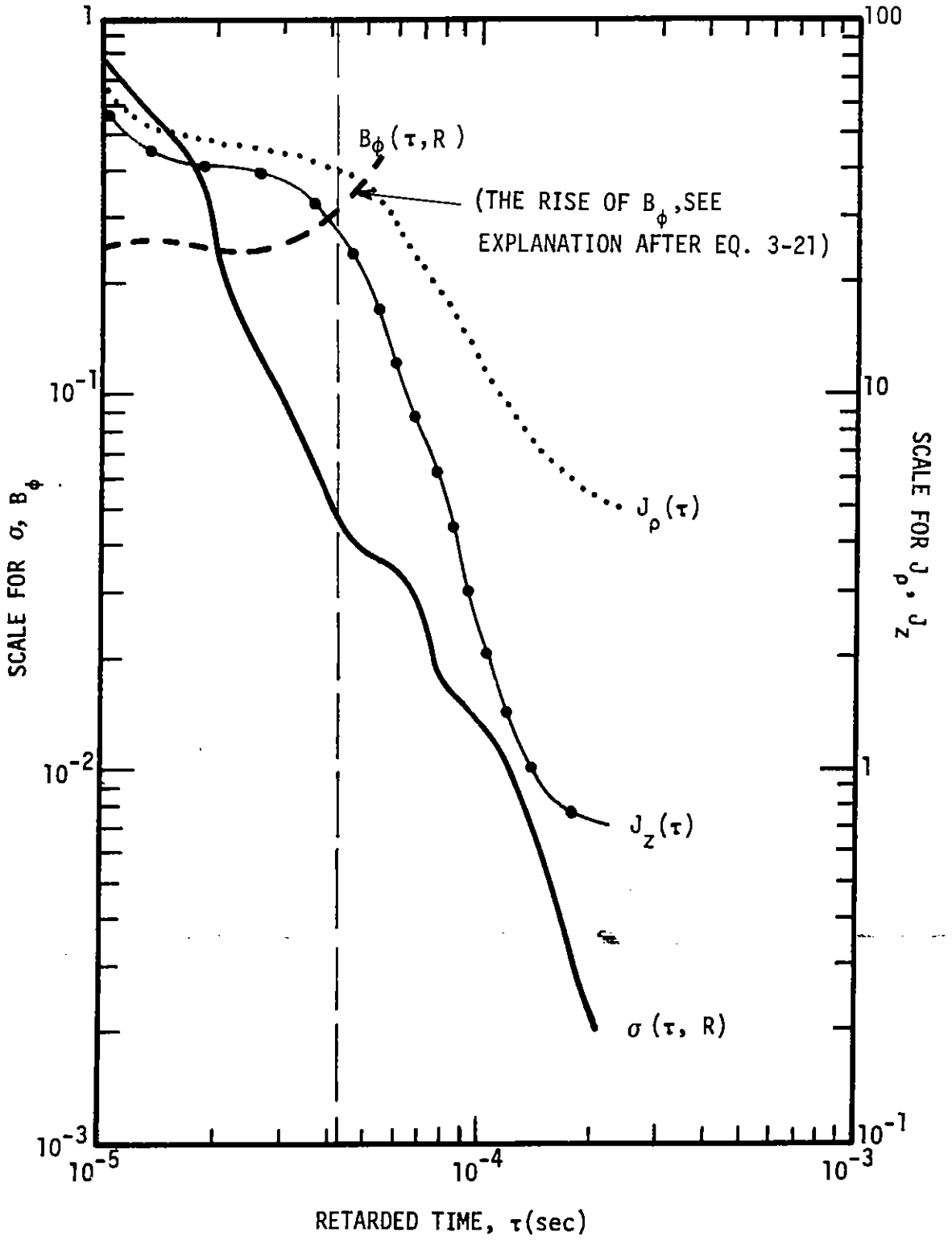

Figure 7. Continuation of Figure 6.

and would probably give a larger effective radius of the wire than its real size and reduce the fields and backflow current on the wire.

SECTION 3

ANALYTICAL RESULTS AND COMPARISON FOR A CONDUCTING WIRE

In this section we solve analytically the wire problem in a source region, evaluate the simple formulas so obtained, and compare them with the previous numerical results from RONDINE. The B_ϕ-correction is ignored in the analysis.

3.1 Simple approximations based on intuition.

We first examine the wire problem intuitively and obtain some simple and crude formulas--to be justified later more carefully. Consider Figure 1. The conductivity σ makes an effective depth $\sim \Delta$ around the wire such that most of the wire's EM effects are confined within this Δ. Physically, this Δ is approximately the skin depth (1-3). If we simply assume that the E_z goes from 0 at $\rho = R$ linearly to $E_{zo} \sim -J_z(\tau)/\sigma$ at $\rho \gtrsim R + \Delta$, then (2-4) with displacement current ignored gives

$$H_\phi(\tau,\rho) = \frac{1}{\rho}\frac{J_z(\tau)}{\Delta}\left[\frac{\rho^3}{3} - \frac{\rho^2(R+\Delta)}{2}\right]_\rho^{R+\Delta}, \quad R \le \rho \le R + \Delta \tag{3-1}$$

where the $J_z(\tau) \sim J_z(\tau,\rho \sim R)$ is assumed to be approximately constant in ρ. Thus, for $R >> \Delta$ we have

$$H_\phi(\tau,R) = \frac{-J_z(\tau)\Delta}{2} \tag{3-2}$$

This gives an intuitively clear interpretation that approximately half the Compton current within Δ flows back through the air conductivity σ, and approximately half flows back on the wire.

For $R << \Delta$, from (3-1) the $H_\phi(\tau,\rho)$ near the wire varies as $1/\rho$. Thus, similarly from (2-4), we have for ρ near R

$$E_z \sim \ell n\ \rho \sim \ell n(\rho/R)\Big/\ell n(R+\Delta)/R \tag{3-3a}$$

and therefore

$$\frac{1}{\rho}\frac{\partial}{\partial\rho}(\rho\ H_\phi) \sim J_z(\tau)\ell n\Big(\rho/(R+\Delta)\Big)\Big/\ell n\Big(R/(R+\Delta)\Big) \equiv f(\rho) \tag{3-3b}$$

Thus, for $R << \Delta$

$$H_\phi(\tau,R) = -\frac{J_z(\tau)\Delta^2}{4R\ \ell n(\Delta/R)} \tag{3-4}$$

Thus, the intuitively clear backflow within Δ onto the wire is reduced by the factor $[\ell n(\Delta/R)]^{-1} \cdot \Delta/(2R)$.

The above results, (3-1) to (3-4), hold only when $\sigma >> \varepsilon\partial/\partial\tau$, with Δ being approximately the skin depth of the main frequency component of the driving current $J_z(\tau)$. Also, the function $f(\rho)$ in (3-3b) approaches $[\rho-(R+\Delta)]/\Delta$ as $R >> \Delta$ and indeed becomes linear and makes (3-1) self-consistent.

To check the detailed analysis, we can also use another simple formula. If we assume

$$\left(\frac{\partial}{\partial\rho}\ E_z(\tau,\rho)\right)_{\rho\ =\ R} = K(\tau)\ E_{zo}(\tau) \tag{3-5}$$

with $K(\tau) \sim \Delta^{-1}$ for $R >> \Delta$ and $K(\tau) \sim \Big(R\ \ell n(\Delta/R)\Big)^{-1}$ for $R << \Delta$, then (2-1) and (2-2) give

$$\mu H_\phi(\tau,R) = \frac{\varepsilon}{\sigma(\tau)}\ K(\tau)\ E_{zo}(\tau) + \int_o^\tau K(\tau)\ E_{zo}(\tau)d\tau \tag{3-6}$$

Equation (3-6) reproduces (3-2) and (3-4) if either of

$$\begin{cases} \sigma J_z(\tau) >> \varepsilon\ \dfrac{\partial}{\partial\tau}\ J_z(\tau) & \text{(3-7a)} \\ \sigma^2 >> \varepsilon\ \dfrac{\partial\sigma}{\partial\tau} & \text{(3-7b)} \end{cases}$$

is true. Equation (3-6) only uses the assumption that the field be linear, and uses the instantaneous skin depth as the scale. It should be more accurate than the fully instantaneous results (3-2) or (3-4) when the "main frequency" of $J_z(\tau)$ is changing with time. This is seen in the numerical comparison in Figure 2.

3.2 The constant conductivity.

If the conductivity does not vary much in the time period considered and does not vary radially, we can treat σ = const. and solve the wire problem by a Laplace transform. For such case, (2-5) for H_ϕ becomes

$$\frac{\partial}{\partial\rho}\left(\frac{1}{\rho}\left[\frac{\partial}{\partial\rho}\,\rho\,H_\phi\right]\right) - \mu\sigma\,\frac{\partial H_\phi}{\partial\tau} = \frac{\partial}{\partial\rho}\,J_z(\tau,\rho) + \frac{1}{c}\,\frac{\partial}{\partial\tau}\,J_\rho(\tau,\rho) \equiv S(\tau,\rho) \qquad (3\text{-}8)$$

Notice that this is a heat diffusion equation with a dissipation or loss term H_ϕ/ρ^2 proportional to the "temperature" H_ϕ and the (radial distance)$^{-2}$. Now the Green's function for (3-8) in the Laplace domain s satisfies

$$\begin{cases} \dfrac{d}{d\rho}\left[\dfrac{1}{\rho}\,\dfrac{d}{d\rho}\,\rho G(s;\rho,\rho')\right] - k^2\,G(s;\rho,\rho') = \dfrac{-\delta(\rho-\rho')}{\rho} & (3\text{-}9a) \\ \left[\dfrac{1}{\rho}\,\dfrac{d}{d\rho}\,(\rho G)\right]_{\rho=R} = 0 & (3\text{-}9b) \\ G(s;\rho,\rho') \xrightarrow[\rho\to\infty]{} 0 & (3\text{-}9c) \end{cases}$$

where $k^2 \equiv \mu\sigma s$. By a straightforward construction, the Green's function $G(s;\rho,\rho')$ is

$$G(s;\rho,\rho') = K_1(k\rho_>)\left[I_1(k\rho_<) + \frac{I_o(kR)}{K_o(kR)}\,K_1(k\rho_<)\right] \qquad (3\text{-}10)$$

where $\rho_>$ and $\rho_<$ are, respectively, the larger and smaller of the two radii ρ and ρ', and K, I are the modified Bessel functions.

Thus, the Laplace transformed $\hat{H}_\phi(s,\rho)$ in the Laplace domain s is

$$\hat{H}_\phi(s,\rho) = -\int_R^\infty d\rho' \rho' \hat{S}(s,\rho') G(s;\rho,\rho') - RG(s;\rho,\rho') \hat{J}_z(s,\rho) \qquad (3\text{-}11)$$

If the $J_z(\tau,\rho)$ is uniform in ρ and the $J_\rho(\tau,\rho)$ due to deflection is ignored, then $S \equiv 0$. In such case the only source of H_ϕ is caused by the boundary condition--the last term in (3-11):

$$\hat{H}_\phi(s,\rho) = \frac{-K_1(k\rho)}{kK_o(kR)} \cdot J_z(s,R) \qquad (3\text{-}12)$$

As a simple case, consider a ρ-independent current

$$J_z(\tau) = J_{zo} e^{\alpha\tau} \qquad (3\text{-}13)$$

Then

$$\hat{H}_\phi(s,\rho) = \frac{-K_1(k\rho)}{kK_o(kR)} \cdot J_{zo} \cdot \frac{1}{s-\alpha} \qquad (3\text{-}14)$$

and the $\hat{H}_\phi(s,\rho)$ in time domain is

$$H_\phi(\tau,\rho) = -J_{zo} e^{\alpha\tau} \frac{K_1(\sqrt{\mu\sigma\alpha}\,\rho)}{\sqrt{\mu\sigma\alpha}K_o(\sqrt{\mu\sigma\alpha}R)} + J_{zo} \int_{\text{Branch cut}} \qquad (3\text{-}15)$$

where the branch cut integral is given in Appendix B.

The limiting expression on the wire for $R\sqrt{\mu\sigma\alpha} >> 1$ is

$$H_\phi(\tau,R) = \frac{-J_{zo} e^{\alpha\tau}}{\sqrt{\mu\sigma\alpha}} \qquad (3\text{-}16)$$

and for $R\sqrt{\mu\sigma\alpha} << 1$ is

$$H_\phi(\tau,R) = \frac{J_{zo}e^{\alpha\tau}}{R(\mu\sigma\alpha)\ \ell n\ (R\sqrt{\mu\sigma\alpha})} \tag{3-17}$$

These check with the intuitively obtained results (3-2) and (3-4), respectively, if we use $\Delta \equiv 2/\sqrt{\mu\sigma\alpha} \equiv \sqrt{2}\delta$ there.

For arbitrary $J_z(\tau,\rho)$ and $J_\rho(\tau,\rho)$, the Laplace transformed $\hat{J}_z(s,\rho)$ and $\hat{J}_\rho(s,\rho)$ must be found and inserted into (3-11). Then the task is to find the inverse transform of (3-11). Unless $\underset{\sim}{J}$ is extremely simple, such an inverse transform is very difficult to evaluate analytically. To simplify the integration procedure for numerical work (3-15) at the surface of the wire can be rewritten as

$$H_\phi(\tau,R) = \frac{-4}{\pi^2 R\mu\sigma}\int_o^\infty du\ \frac{e^{-\frac{\tau u^2}{R^2\mu\sigma}}}{uH_o^{(1)}(u)\ H_o^{(2)}(u)}\int_o^\tau J_z(R,\tau')\ e^{\frac{\tau' u^2}{R^2\mu\sigma}}\cdot d\tau' \tag{3-18}$$

where $H_o^{(1)}$, $H_o^{(2)}$ are, respectively, Hankel functions of the first and second kind with zero order [5]. If $J_z(\tau)$ is simple enough for the τ'-integration to be carried out, it leaves only a one-dimensional integration over u to be done numerically. For example, a constant $J_z(\tau) = J_{zo}U(\tau)$ where $U(\tau)$ is a step function, gives

$$H_\phi(\tau,R) = J_{zo}\frac{-4R}{2}\int_o^\infty \frac{(1-e^{\frac{-\tau u^2}{R^2}})du}{u^3 H_o^{(1)}(u)H_o^{(2)}(u)} \tag{3-19}$$

$$\xrightarrow[\tau >> R^2\mu\sigma]{} \frac{-2\tau J_{zo}}{\mu R\sigma\ell n\frac{\tau}{R^2\mu\sigma}}$$

which increases without limit as it should when $\tau \to \infty$. As another example, if $J_z(\tau)$ only lasts from $0 \leq \tau \leq \Delta\tau$, then for $\tau > \Delta\tau$

$$H_\phi(\tau,R) = \frac{-4}{\pi^2 R\mu\sigma}\int_o^\infty du\ \frac{e^{\frac{-\tau u^2}{R^2\mu\sigma}}}{uH_o^{(1)}(u)H_o^{(2)}(u)}\int_o^{\Delta\tau} d\tau'\ e^{\frac{\tau' u^2}{R^2\mu\sigma}}\ J_z(\tau') \qquad (3\text{-}20)$$

which goes to zero as $\tau \to \infty$ as

$$\begin{cases} H_\phi(\tau,R) \xrightarrow[\tau \to \infty]{} \dfrac{2}{R\mu\sigma\ell n\left(\dfrac{\tau}{R^2\mu\sigma}\right)}\displaystyle\int_o^{\Delta\tau} d\tau'\ e^{\frac{\tau'}{\tau}}\ J_z(\tau') \\ \\ \tau >> \Delta\tau,\ R^2\mu\sigma \end{cases} \qquad (3\text{-}21)$$

This shows that the decaying of H_ϕ after the elapse of $J_z(\tau)$ is extremely slow. The test case of a constant $J_z(\tau)$ with short duration $\Delta\tau$ and a constant σ is used to run RONDINE as a check. The RONDINE numerical B_ϕ value shows a remarkable agreement, as predicted by (3-20) and (3-21). This test case is plotted in Figure 8.

Also, it is important to notice explicitly that there are two different effects caused by a time varying conductivity $\sigma(\tau)$ on the B_ϕ or the backflow current I on the wire. First, a slowly decreasing (increasing) $\sigma(\tau)$ long <u>after</u> a source driving current $J_z(\tau_{early})$ has passed makes the rate of decay of that part of B_ϕ caused by that $J_z(\tau_{early})$ become faster (slower) logarithmically, according to (3-21) and the following (3-24). Second, a smaller (larger) $\sigma(\tau)$ <u>while</u> the source driving current $J_z(\tau_{while})$ is producing its magnetic field makes an inversely proportionally stronger (weaker) $B_\phi(\tau_{while})$ produced by that $J_z(\tau_{while})$, according to (3-19). Thus, by linear superposition, a <u>late-time sustained source</u>

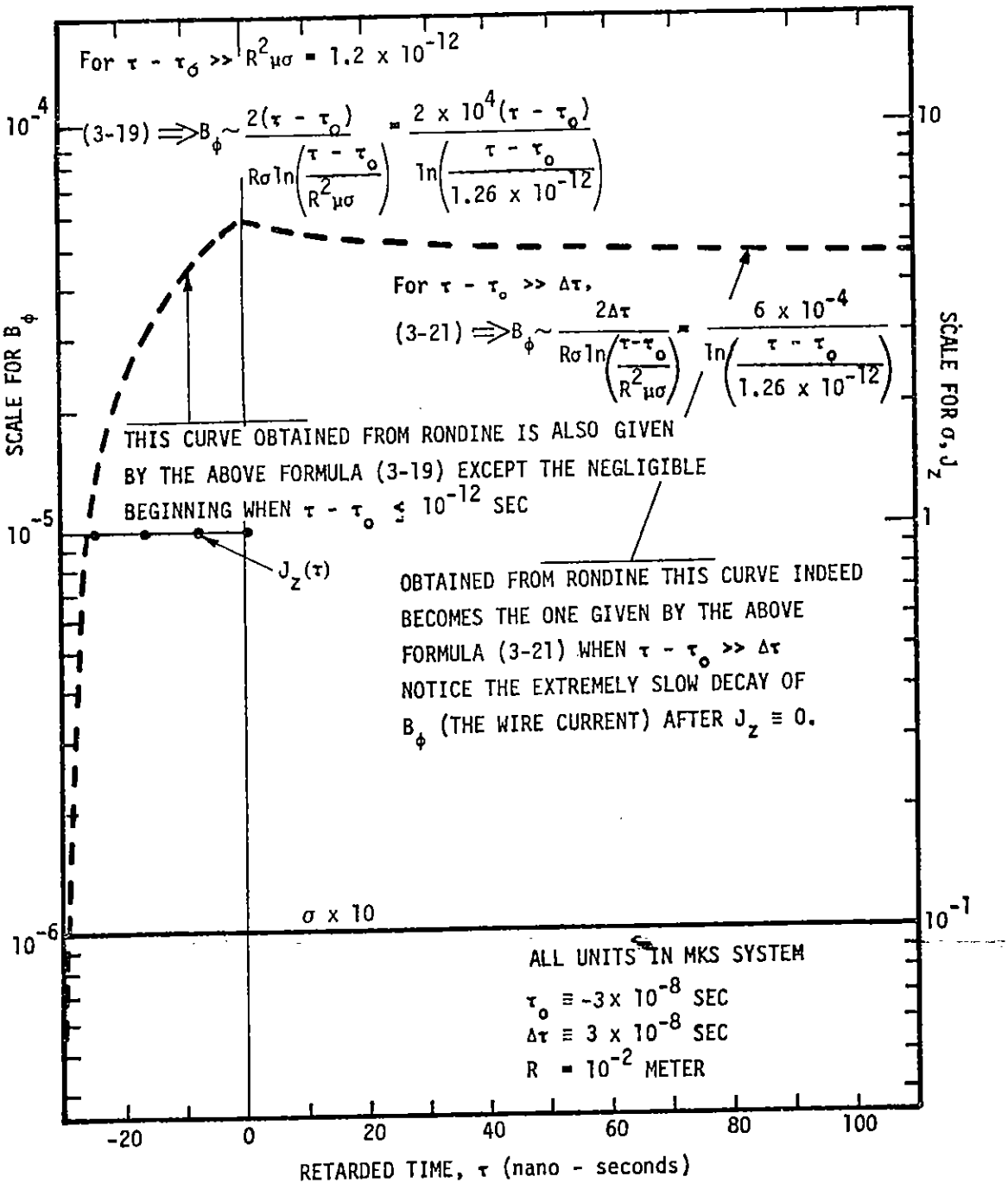

Figure 8. Comparison of RONDINE and theoretical analysis for the test problem.

current $J_z(\tau)$, combined with a decreasing late-time $\sigma(\tau)$, can produce a larger B to offset the faster decay of the B left by early $J_z(\tau_{early})$ and makes the total B_ϕ increase. This explains the late-time B_ϕ increases of RONDINE output noted in the previous section as being caused by $J_z(\tau)$ and $\sigma(\tau)$ at late times $\left(\geq 3 \times 10^{-5} \text{ sec} \right)$ [7].

3.3 Large and slowly changing conductivity $\sigma(\tau)$.

If the conductivity $\sigma(\tau)$ is time dependent, but is large and changes slowly, the equation for H_ϕ reduces to the diffusion equation, with an equivalent "sink loss" term. There are two physical situations that satisfy the "largeness" and "slowness" of $\sigma(\tau)$:

$$\sigma^2 >> |\sigma' \epsilon|, \quad \sigma' \equiv d\sigma/d\tau. \tag{3-22a}$$

or

$$\left| \frac{\frac{\partial}{\partial \tau} \underset{\sim}{J}}{J} \right| >> \left| \frac{\sigma'}{\sigma} \right| \tag{3-22b}$$

The first one is satisfied when the fractional change of the conductivity is small during the relaxation time of that conductivity, and the second is satisfied when the driving current is changing much faster than the conductivity. The source region problem satisfies (3-22a) all the time.

Under the condition (3-22a), (2-5) becomes

$$\frac{\partial}{\partial \rho} \left[\frac{1}{\rho} \frac{\partial}{\partial \rho} \left(\rho H_\phi(\tau,\rho) \right) \right] - \mu\sigma(\tau) \frac{\partial}{\partial \tau} H_\phi = \frac{\partial}{\partial \rho} J_z(\tau,\rho) + \frac{\sigma(\tau)}{c} \frac{\partial}{\partial \tau} \left[\frac{J_\rho(\tau,\rho)}{\sigma(\tau)} \right] \tag{3-23}$$

The condition (3-22b) yields the same equation except that the source (3-8) replaces the right-hand source term in (3-23). The solution for (3-23) can be easily obtained similar to the constant σ case, except that we first change the time variable

$$dT = \frac{d\tau}{\sigma(\tau)/\sigma_o} \quad \text{or} \quad T = \int_{\tau_o}^{\tau} \frac{\sigma_o d\tau}{\sigma(\tau)} \tag{3-24}$$

where σ_o is a convenient constant conductivity in the problem for the normalization purpose. Then in terms of the new independent variable (T,ρ), (3-23) becomes

$$\frac{\partial}{\partial\rho}\left(\frac{1}{\rho}\frac{\partial}{\partial\rho}\rho H_\phi\right) - \mu\sigma_o \frac{\partial}{\partial\tau} H_\phi = S_1(T,\rho) \tag{3-25}$$

and can be solved exactly as for the constant σ case in Section 3.2. Notice that (3-24) simplifies (3-23) into (3-25) only when $\sigma = \sigma(\tau) = \sigma(t-z)$ but is uniform in ρ.

As a simple example, consider a conductivity

$$\sigma(\tau) = \sigma_o e^{\beta\tau} \tag{3-26}$$

with its accompanying time variable change

$$T = \frac{e^{-\beta\tau}}{-\beta}, -\infty < \tau < \infty, \quad -\infty < T < 0 \tag{3-27}$$

and a simple rising source current

$$J_z(\tau) = J_o e^{\alpha\tau} = \frac{J_o}{(-\beta T)^{\alpha/\beta}} \equiv J(T) \tag{3-28}$$

Notice, of course, this includes the case that $\sigma(\tau)$ and $J_z(\tau)$ rise with the same pace, i.e., the $\alpha = \beta$ case. Now Equations (3-13) to (3-17) can be used immediately, except with the replacement $\sigma \to \sigma_o$ and $\alpha \to \alpha_{eq}$. A rough estimate for the α_{eq} is obtained by using the instantaneous derivative of $J(T)$

$$\frac{\partial}{\partial T} J(T) = J(T) \frac{\alpha}{-\beta T} \tag{3-29}$$

which gives

$$\alpha_{eqo} \equiv \frac{\alpha}{-\beta T} = \alpha e^{\beta\tau} \tag{3-30}$$

Using this α_{eqo} and σ_o is exactly substituting the instantaneous $\sigma(\tau)$ into the results for the case of constant σ. The result so obtained for $|H_\phi|$ is larger than the actual one, because the instantaneous α_{eqo} is too high. A better approximation is achieved by averaging down the value of α_{eq} for $\tau > 0$ by

$$\alpha_{eq1} = \frac{1}{T + \frac{1}{\beta}} \int_{\frac{1}{-\beta}}^{T} \frac{\alpha}{-\beta T'} dT' = \alpha e^{\beta\tau} \frac{\beta\tau}{e^{\beta\tau} - 1} \tag{3-31}$$

The α_{eq1} and the σ_o can be used in (3-13) to (3-17) under the conditions

$$\sigma_o << \beta\varepsilon \qquad \text{(small initial } \sigma_o\text{)} \tag{3-32a}$$

$$\beta\tau \lesssim 1 \qquad \text{(non-early time)} \tag{3-32b}$$

$$\sigma(\tau) >> \alpha\varepsilon \qquad \text{(large conductivity)} \tag{3-32c}$$

where $\sigma_o \equiv \sigma(\tau = 0)$ is chosen at the earliest time that both $\sigma(\tau)$ and $J(\tau)$ start behaving as (3-26) and (3-28), respectively, and satisfy (3-32).

3.4 Comparison with RONDINE.

Using (3-17) and (3-31) for the rising period of the RONDINE current and conductivity, the B_ϕ obtained by this simple theoretical formula is plotted in Figure 2 in the time duration when it is applicable. It shows very good agreement with the RONDINE computed B_ϕ. At the time (3-32) does not hold, we continue the curve by formula (3-6), using $1/\tau$ for the frequency in the skin depth and neglecting the first term at its right-hand side.

Now the rising period behavior and the late-time behavior of RONDINE show agreement with analytical predictions. Evidently, it is a valid numerical code for cylindrical source region problems.

SECTION 4

OTHER CIRCULAR CYLINDRICAL GEOMETRY

4.1 Coaxial region.

To account for the ground's effect roughly when the wire is many skin depths above it, and for future references, we include here the solution for a source region between two coaxial conductors at cylindrical radius $\rho = R$ and $\rho = R_{out}$, and with a constant conductivity. The Green's function, instead of the (3-10) for a bare wire, becomes

$$G(s,\rho,\rho') = \frac{\left[I_1(k\rho_>) \frac{K_o(kR_{out})}{I_o(kR_{out})} + K_1(k\rho_>) \right] \left[I_1(k\rho_<) + \frac{I_o(kR)}{K_o(kR)} K_1(k\rho_<) \right]}{1 - \frac{I_o(kR)\, K_o(kR_{out})}{I_o(kR_{out})\, K_o(kR)}} \tag{4-1}$$

in the Laplace domain s, where $k \equiv \sqrt{\mu\sigma s}$ as before.

If the driving current $J_z(\tau)$ is independent of ρ, then instead of (3-12), we have

$$\hat{H}_\phi(s,\rho) = \frac{-\left[K_1(k\rho) + \frac{K_o(kR_{out})}{I_o(kR_{out})} I_1(k\rho) \right] \hat{J}_z(s)}{k\, K_o(kR) \left\{ 1 - \frac{I_o(kR)\, K_o(kR_{out})}{I_o(kR_{out})\, K_o(kR)} \right\}} \tag{4-2}$$

For the code RONDINE, the only difference the coaxial region makes is to replace the boundary condition B. 7 at p. 35 of ONDINE for $\rho = \rho_\infty$ ($j = J$ for the grid number) by

$$H_J = \frac{F_{J-1} - j_X(J-1) \cdot \Delta Z_{J-1,J} \cdot \frac{Z(J) + Z(J-1)}{2}}{1 - E_{J-1}} \tag{4-3}$$

as a result of replacing the second of Equation (2-8) by

$$\left(\frac{1}{\rho}\frac{\partial}{\partial\rho}\rho H_\phi(\tau,\rho)\right)_{\rho=R_{out}} = J_z\left(\tau,R_{out}\right) \qquad (4\text{-}3')$$

4.2 Underground test EMP prediction.

For an underground test, the EMP in a circular cylindrical air conduit surrounded by coaxial concrete layers and parallel to the incident γ-flux can be obtained by RONDINE. The only change needed is to replace (2-12) at the wire by

$$E_1 = 0$$
$$F_1 = 0 \qquad (4\text{-}4)$$

at the center, and use (4-3) at the outer conducting enclosure that encloses the concrete. Also, of course, the driving Compton current is now in the center air conduit only.

REFERENCES

1. W. J. Karzas and R. Latter, Air Conductivity Produced by Nuclear Explosions, The Rand Corporation, RM-3671-PR, May 1963.

2. C. L. Longmire, Theory of EMP from Nuclear Surface Bursts, Los Alamos Nuclear Corporation, LANC-R-6, January 1970.

3. C. E. Baum (ed.), EMP Interaction Notes, (see for many interesting papers).

4. W. R. Graham and E. R. Parkinson, ONDINE: A Numerical Solution to Maxwell's Equations in One Dimension, The Rand Corporation, R-701-DASA, February 1971.

5. R. Richtmyer and K. Morton, Difference Methods for Initial Value Problems, John Wiley and Sons, 2nd ed., 1967, p. 198.

6. Handbook of Mathemetical Functions, National Bureau of Standards, AMS 55, edited by M. Abramowitz and I. A. Stegun, 1964.

7. D. Sargis, E. Parkinson, J. Wood, R. Dietz, C. Stevens, Late Time Sources for Close-In EMP, DNA-3064F, SAI-72-556-LJ, August 1972.

8. C. T. C. Mo, Analysis of the Response of a Conductor Immersed in an EMP Source Region - The Steady State, R & D Associates, RDA-TR-2301-009, December 1973.

APPENDIX A
RONDINE GRID SIZES

Concerning the increment grid sizes, we use an exponentially increasing grid for both $\Delta\tau$ and ΔZ to take into account the fast change of the fields in the early times and near the wire. The scheme we used for Z is

$$Z(j) = R + (\Delta Z)_0 \left(10^{(j-1)/M_Z} - 1\right) \tag{A-1}$$

$j = 1, 2, \ldots, (N_{air} + 1)$; $N_{air} \equiv$ number of layers in the air

where the scale factor M_Z is determined by the farthest distance ρ_∞ of Equation (2-9) such that

$$\rho_\infty = R + (\Delta Z)_0 \cdot \left(10^{N_{air}/M_Z}\right) - 1 \tag{A-2}$$

which gives

$$M_Z = \frac{N_{air}}{\log_{10}\left(\frac{\rho_\infty - R}{(\Delta Z)_0} + 1\right)} \tag{A-3}$$

This increment scheme yields a successive grid size ratio

$$\frac{\Delta Z(j)}{\Delta Z(j-1)} = \left[1 + \frac{\rho_\infty - R}{(\Delta Z)_0}\right]\frac{1}{N_{air}} \tag{A-4}$$

that is a constant greater than or equal to 1, and controls the first grid size for j = 1 to j = 2 to be

$$\Delta Z(1) = (\Delta Z)_o \left[\left(1 + \frac{\rho_\infty - R}{(\Delta Z)_o} \right)^{\frac{1}{N_{air}}} - 1 \right]$$

$$= (\Delta Z)_o \frac{\ln \left(1 + \frac{\rho_\infty - R}{(\Delta Z)_o} \right)}{N_{air}} \quad \text{if } N_{air} >> \ln \left(1 + \frac{\rho_\infty - R}{(\Delta Z)_o} \right) \tag{A-5}$$

The advantage of this scheme is that we can first fix the ρ_∞ where the integration is desired to be carried to, then we can choose any "basic" size $(\Delta Z)_o$ and number of grid N_{air} and always have the integration carried to the fixed ρ_∞. Further, the basic size $(\Delta Z)_o$ controls the monotonically increasing grid size from being almost uniform to being highly non-uniform, as (A-4) clearly shows.

The time increment is treated similarly. We use

$$\begin{cases} T(n) = T_o + (\Delta T)_o \left[10^{\frac{n-1}{M_T}} - 1 \right] \\ n = 1, \ldots, (n_{steps} + 1) \end{cases} \tag{A-6}$$

where n_{steps} is the total number of time steps and M_T is the scale factor given by

$$M_T = \frac{n_{steps}}{\log_{10} \left(\frac{T_{max} - T_o}{(\Delta T)_o} + 1 \right)} \tag{A-7}$$

APPENDIX B

INTEGRAL (3-15)

The branch cut integral in (3-15), with $s^{1/2} = r^{1/2} e^{i\theta/2}$, $\pi < \theta < \pi$ along the negative real axis, integrated on the path shown in the sketch below has the value

$$\int_{\text{Branch cut}} = \frac{i}{2\pi} \int_o^\infty dr\, e^{-r\tau} \frac{1}{(r+\alpha)\sqrt{\mu\sigma r}} \left[\frac{H_1^{(1)}(\sqrt{\mu\sigma r}\rho)}{H_0^{(1)}(\sqrt{\mu\sigma r}R)} - \frac{H_1^{(2)}(\sqrt{\mu\sigma r}\rho)}{H_0^{(2)}(\sqrt{\mu\sigma r}R)} \right] \tag{B-1}$$

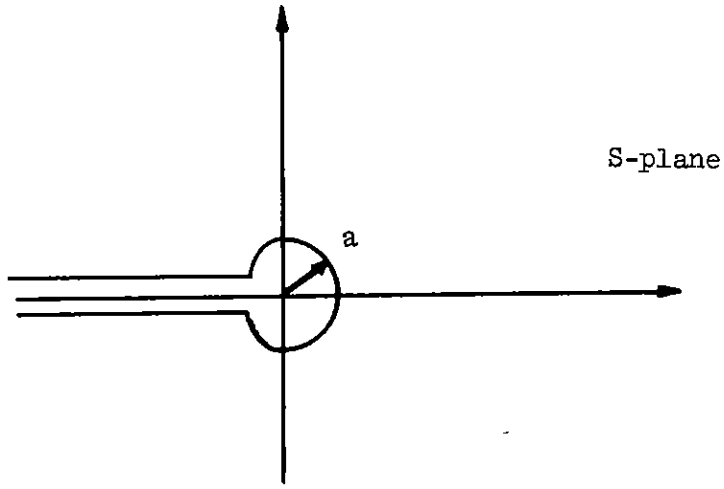

On the wire surface $\rho = R$, then

$$I \equiv \int_{\substack{\text{Branch cut,} \\ \text{on } \rho = R}} = \frac{2}{\pi^2} \int_o^\infty dr\, \frac{e^{-r\tau}}{r+\alpha} \frac{1}{R\mu\sigma r} \frac{1}{H_0^{(1)}(\sqrt{\mu\sigma r}\, R)\, H_0^{(2)}(\sqrt{\mu\sigma r}\, R)}$$

$$= \frac{4R}{\pi^2} \int_o^\infty \frac{e^{\frac{-\tau}{R^2\mu\sigma} x^2}\, dx}{x(x^2 + R^2\mu\sigma\alpha)\, H_0^{(1)}(x)\, H_0^{(2)}(x)} \tag{B-2}$$

Now the $H_0^{(1)}(x)\ H_0^{(2)}(x) \equiv J_0^2(x) + Y_0^2(x) \sim [\ell n(x)]^2$ as $x \to 0$ and $\sim 2/(\pi x)$ as $x >> 1$ can be used to approximate (B-2). Thus, we can approximate I by

$$I = \frac{4R}{2\pi^2} \int_0^\infty \frac{e^{\frac{-\tau}{R^2\mu\sigma} x^2} \pi x}{x(x^2 + R^2\mu\sigma\alpha)}\, dx = \frac{e^{\alpha\tau}}{\sqrt{\mu\sigma\alpha}} \left[1 - \text{erf}\ (\alpha\tau)\right] \qquad \text{(B-3)}$$

Thus, for $R\sqrt{\mu\sigma\alpha} >> 1$, (B-3) gives (3-16) if $\alpha\tau$ is not $<< 1$. For $R\sqrt{\mu\sigma\alpha} << 1$, (B-3) contributes a term of the order $R\sqrt{\mu\sigma\alpha}\ \ell n\ (R\sqrt{\mu\sigma\alpha})$ smaller compared with the limit of the first term of (3-15), and results in (3-17).